Article

Petrogenesis of Late Cretaceous Muscovite-Bearing Peraluminous Granites in the Youjiang Basin, South China Block: Implications for Tin Mineralization

Ping Li [1], Xijun Liu [1,2,3,*] and Lei Liu [1,*]

[1] Guangxi Key Laboratory of Hidden Metallic Ore Deposits Exploration, College of Earth Sciences, Guilin University of Technology, Guilin 541004, China; leeping14@163.com

[2] Collaborative Innovation Center for Exploration of Nonferrous Metal Deposits and Efficient Utilization of Resource, Guilin University of Technology, Guilin 541004, China

[3] National Key Laboratory of Ecological Security and Resource Utilization in Arid Areas, Xinjiang Institute of Ecology and Geography, Chinese Academy of Sciences, Urumqi 830011, China

* Correspondence: xijunliu@glut.edu.cn (X.L.); liulei@glut.edu.cn (L.L.);
  Tel.: +86-152-7739-5399 (X.L.); +86-159-7734-6062 (L.L.)

Abstract: Most primary Sn deposits worldwide are associated with muscovite-bearing peraluminous granites, commonly believed to originate from the partial melting of metasedimentary rocks. We studied the whole-rock geochemistry and Sm–Nd isotopes of Late Cretaceous (~90 Ma) Laojunshan muscovite-bearing peraluminous granites in the Youjiang Basin, South China Block. The globally significant Dulong tin mineralization was co-genetic with the Laojunshan muscovite-bearing monzogranites. The Laojunshan granites exhibit slightly higher εNd(t) values than the Precambrian basement, indicating a hybrid crustal source comprising both Precambrian rock and juvenile components. Characterized by weakly peraluminous compositions, these granites display highly evolved geochemical features: notably low levels of Ca, P, Mg, Fe, and Ti contents, elevated Si content, a high FeO^T/MgO ratio, and a low Zr/Hf ratio. These distinctive geochemical features can be attributed to the differentiation of plagioclase, biotite, and zircons, with the remarkably low Nb/Ta and K/Rb ratios further suggesting a fluid exsolution process. The geochemical data propose that tin-enriched Laojunshan granites originate from mineral differentiation and fluid exsolution of crust-derived melts during magmatic evolution. By integrating these novel findings with existing data on coeval muscovite-bearing granites co-genetic with tin mineralization in the Youjiang Basin, it is deduced that these granites share a unified origin. Their genesis can be attributed to mineral differentiation and fluid exsolution of crust-derived melts rather than a direct melting of metasedimentary rocks.

Keywords: muscovite-bearing granite; minerals differentiation; fluid exsolution; Late Cretaceous; Youjiang Basin

1. Introduction

Most primary Sn deposits worldwide are related to peraluminous granitoids [1–3]. Peraluminous granitoids, with respect to mineral and rock associations, can be categorized into two types: biotite-rich tonalites to monzogranites and muscovite-bearing monzogranites to alkali-feldspar granites [4,5]. Biotite-rich and muscovite-bearing peraluminous granites constitute the prevailing magmatic rocks within tin polymetallic metallogenic belts [1,3,5]. Previous studies have indicated that Sn mineralization is only closely associated with muscovite-bearing granites and not with biotite-rich granites [3,6,7]. Muscovite-bearing peraluminous granites connected to tin mineralization are believed to originate from the partial melting of metasedimentary rocks [3,6,8–10]. While Barbarin (1996) [4] proposed that muscovite-bearing peraluminous granites arise from "wet" anatexis of crustal rocks at relatively low temperatures, experimental melts derived from metasedimentary rocks by

H_2O-fluxing are tonalitic with low K/Na ratios, differing in composition from muscovite-bearing peraluminous granites [11,12]. Furthermore, there remains considerable debate concerning the mechanism of tin enrichment in granitic magmas. Earlier studies demonstrated that tin accumulates in most evolved granitic magmas during magma evolution, as revealed by TiO_2-Sn, Rb/Sr-Sn, and TiO_2/Ta-Sn binary covariant diagrams [13,14]. Romer and Kroner (2015) [8] identified a 3000 km long Late Paleozoic tin-tungsten mineralization in the Acadian, Variscan, and Alleghanian orogenic belts of Europe and Atlantic Northern America. They proposed that these large tin deposits occurred solely in regions where the Sn-enriched weathered sediments redeposit. Thus, the formation of tin-bearing granites might be associated with tin enrichment in sedimentary source. Recently, by comparing element partitioning between leucosomes and resites of high- and low-temperature migmatites, Wolf et al. (2018) [10] suggested that the complete biotite consumption of high-temperature (>800 °C) anatexis can produce tin-rich granites without extreme differentiation.

Late Cretaceous muscovite-bearing peraluminous granites are widespread in the Youjiang Basin of the South China Block. They are associated with several world-class or large tin-polymetallic deposits, including the Dulong, Bainiuchang, Gejiu, Mangchang, and Dachang deposits [7,15–18]. These granites offer a remarkable opportunity to investigate the origin of the muscovite-bearing peraluminous granitic melts. This study presents the whole-rock major and trace element and Sm–Nd isotopic compositions of the Laojunshan muscovite-bearing peraluminous granites that produced the Dulong tin-polymetallic deposit. Our approach is rooted in the understanding that the granite's composition variation is controlled by both the source and the process of magmatic evolution. The primary objectives of this research are to (1) elucidate the petrogenesis of the Laojunshan muscovite-bearing granites, (2) identify the principal factor governing tin enrichment in the Laojunshan granites.
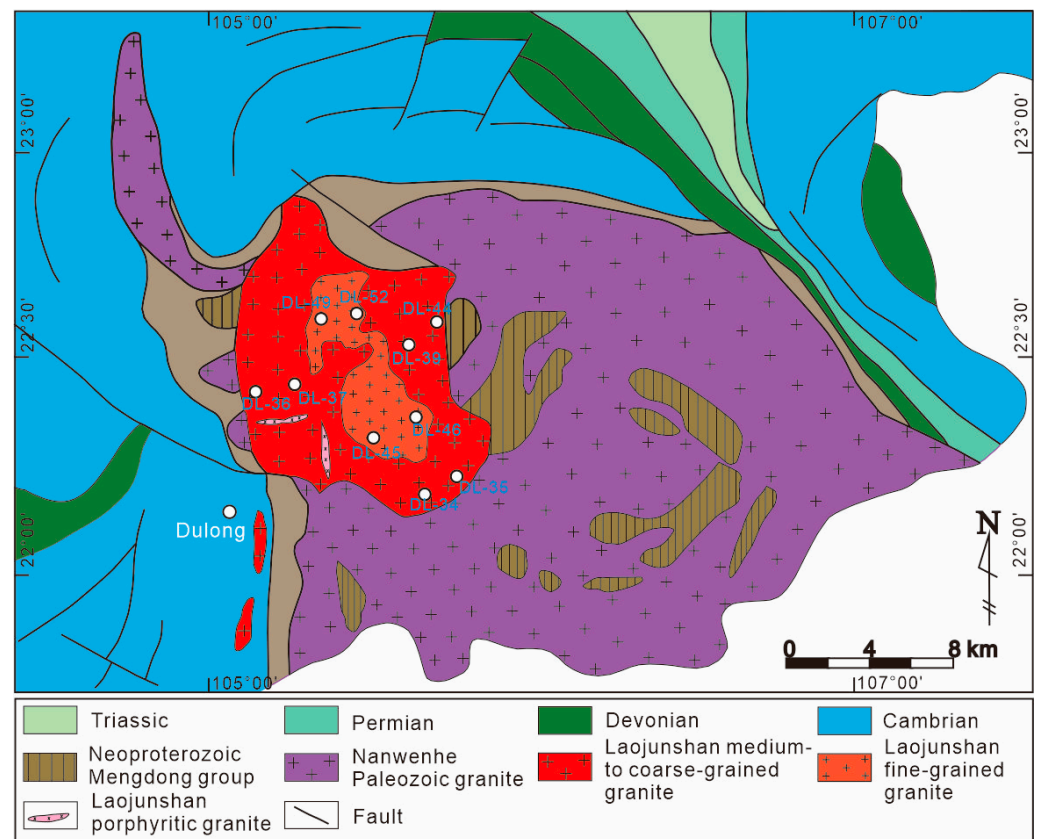
2. Geological Setting and Sampling

The Youjiang Basin is situated in the southwestern part of the South China Block (Figure 1a). The exposed Precambrian basement in the Youjiang Basin comprises Paleoproterozoic granulites, amphibolites, gneisses, and schists, as well as Neoproterozoic flysch turbidites and Early Paleozoic sandstone, siltstone, mudstone, limestone, and dolomite [19]. These strata are overlain by Late Paleozoic–Early Mesozoic carbonates and terrigenous clastic rocks [17] (Figure 1b). Late Cretaceous magmatic rocks are widely distributed within an extensional setting linked to the Neo-Tethyan or Paleo-Pacific subduction [7,19–22]. These rocks encompass dominant granites, secondary gabbros, mafic enclaves, and alkaline syenites [7]. Characterized by peraluminous compositions, these granites fall into two types: muscovite-bearing and biotite-rich. Muscovite-bearing peraluminous granites encompass intrusions such as the Laojunshan, Bozhushan (episode 2), Kafang–Laochang, Gaofengshan, Songshujiao, Longxianggai, and Mangchang intrusions, which correspond to the Dulong, Bainiuchang, Gejiu, Dachang, and Mangchang tin-polymetallic deposits [7,9,23–25] (Figure 1b). In contrast, the biotite-rich granites include the Shenxianshui, Bozhushan (episode 1), Jiasha, and Longchahe intrusions, which lack Sn deposits [7,26]. The Kafang-Laochang, Gaofengshan, Songshujiao, Shenxianshui, Jiasha, and Longchahe intrusions are exposed in the Gejiu area [27]. Zircon U-Pb dating establishes the Late Cretaceous emplacement of both muscovite-bearing granites and biotite-rich granites were emplaced during the Late Cretaceous [7,19]. Additionally, these Late Cretaceous granites display also similar whole-rock Sm-Nd and zircon Lu-Hf isotopic ratios, excluding the Laojunshan granites [7,19,20,28].
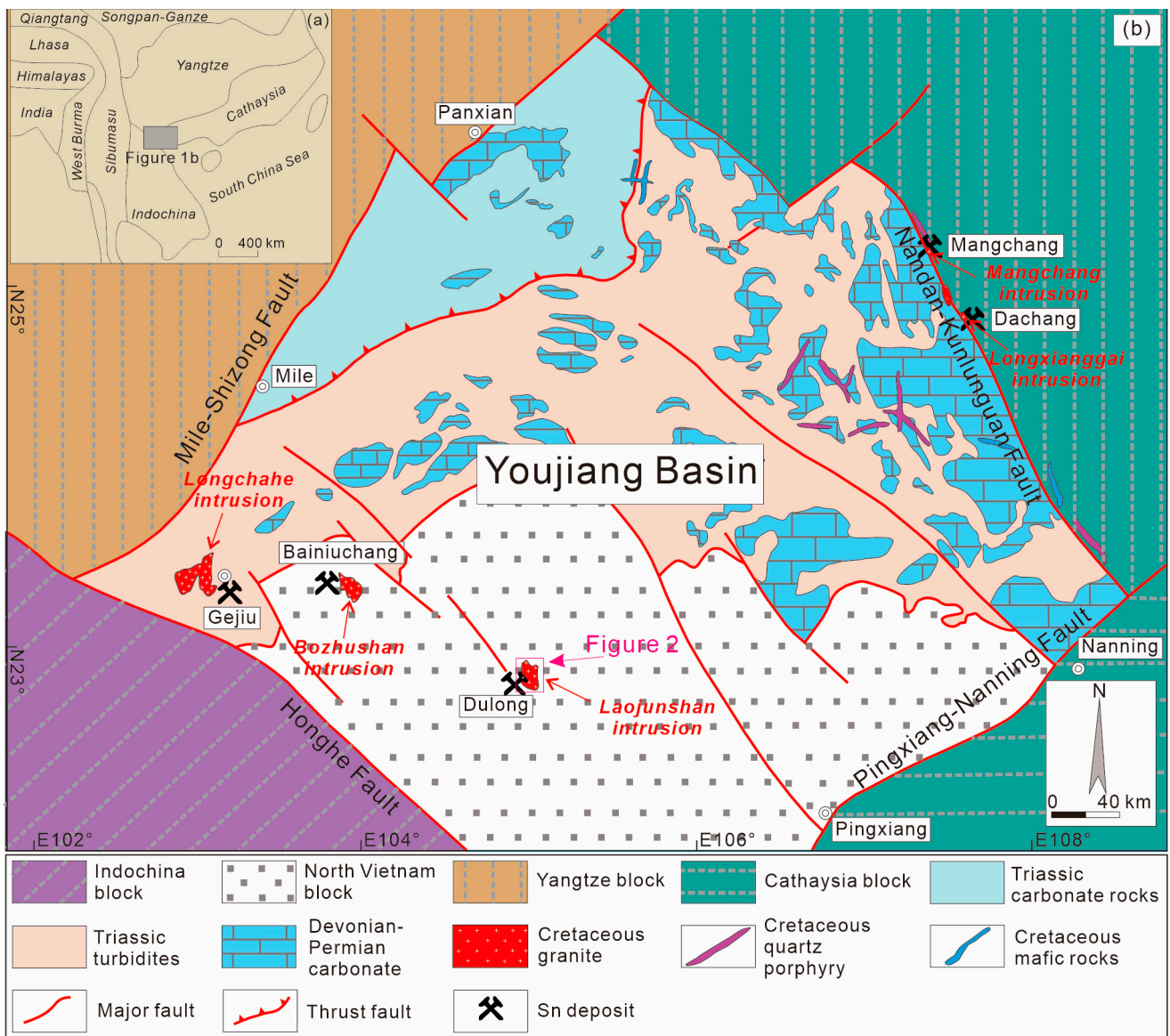
Figure 1. (**a**) Simplified tectonic framework of the South China Block and surrounding areas; (**b**) geological map showing the distribution of Late Cretaceous granitic intrusions and tin ore fields in the Youjiang Basin [7,20].

The Laojunshan granitic batholith is situated on the northeastern side of the Dulong tin-polymetallic deposit (Figure 2), intruding into the Neoproterozoic Mengdong Group and Late Paleozoic Nanwenhe granitic batholith [29] (Figure 2). Covering an approximate surface area of 134 km^2, the Laojunshan granitic batholith's subsurface extension has been revealed through drilling data, extending beneath the Dulong Sn deposit [30].

Figure 2. Geological map and sampling location of the Laojunshan intrusion (modified after [9]).

The batholith encompasses three intrusive granitic suites: medium- to coarse-grained monzogranite, fine-grained monzogranite, and porphyritic granite. Laser ablation-inductively coupled plasma-mass spectroscopy (LA–ICP–MS) zircon U-Pb dating of these granitic suites provide ages of 90.1 ± 0.7, 89.7 ± 0.8, and 86.0 ± 0.5 Ma [9]. According to LA-ICP-MS zircon U-Pb dating conducted by [31], the coarse-grained monzogranites and fine-grained monzogranites are formed between 85.6 ± 0.8 Ma and 90.4 ± 0.7 Ma and at 89.9 ± 1.4 Ma, respectively. SHRIMP zircon U-Pb dating of the coarse monzogranites yielded an age of 83.3 ± 1.5 Ma [32]. Drawing from compiled data from previous studies and new age data obtained through LA-MC-ICPMS U-Pb dating, Lan et al. (2016) [33] concluded that the Laojunshan granitic batholith resulted from three magmatic episodes: 80–88 Ma, 90–98 Ma, and 100–118 Ma.

The medium- to coarse-grained and fine-grained monzogranites exhibit the typical granitic texture of granite. They comprise plagioclase (~15%–20%), K-feldspar (~30%–35%), quartz (~30%–40%), muscovite (~5%), and biotite (~2%) (Figure 3). Accessory minerals include titanite, apatite, zircon, and sphene. LA–ICP–MS U-Pb dating of cassiterites from the Dulong deposit indicates a $^{207}Pb/^{206}Pb–^{238}U/^{206}Pb$ concordia age of 89.4 ± 1.4 Ma, implying a co-genetic association of tin mineralization with the Laojunshan muscovite-bearing monzogranites [18]. For this study, we selected six medium- to coarse-grained and four fine-grained muscovite-bearing monzogranites from the Laojunshan batholith for whole-rock major elements, trace elements, and Sm–Nd isotopic analyses. The respective sampling locations are depicted in Figure 2.
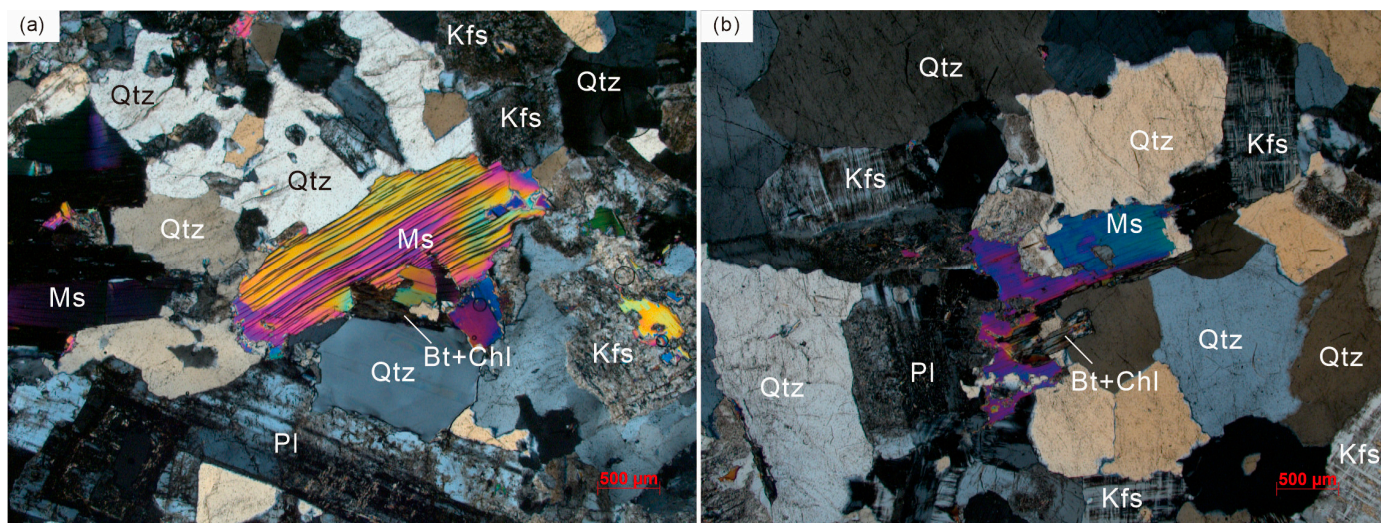
Figure 3. Representative photomicrographs of the Laojunshan muscovite-bearing peraluminous granites. (**a**) Medium to coarse-grained monzogranite (episode 1); (**b**) fine-grained monzogranite (episode 2). Notes: Pl, plagioclase; Kfs, K-feldspar; Bt, biotite; Qtz, quartz; Ms, muscovite; Chl, chlorite.

3. Analytical Methods

The major element compositions were determined through inductively coupled plasma–optical emission spectrometry (ICP–OES; Agilent 720) (Agilent Technologies Inc., Palo Alto, CA, USA) and was employed at the Guangzhou Tuoyan Analytical Technology Company (GTATC) in Guangzhou, China. The analytical precision was estimated to be $\pm 2\%$ for major elements with contents >0.5 wt.%, and $\pm 5\%$ for minor elements with contents ranging from 0.1 to 0.5 wt.%. For the analysis of trace element compositions, a Jena Plasma Quant ICP–MS (Jena Inc., Jena, Germany) was employed. About 0.05 g of the powdered sample was introduced into a PTFE bomb containing 0.6 mL HF and 3 mL HNO_3. The sealed bombs were subjected to heating at 185 °C for approximately 36 h. Post-cooling, the bombs were dried using a hot plate. Subsequently, 200 ng of Rh (used as an internal standard) [7], 2 mL of HNO_3, and 4 mL of water were added to the sample. The sealed bombs were once again sealed and placed in an oven at 135 °C for approximately 5 h to dissolve any remaining residues. Following cooling, the final dilution factor for ICP–MS analysis was approximately 3000. The accuracy was assessed to be $\pm 5\%$ for most trace elements.

The Sm-Nd isotope analysis was conducted at the Guangzhou Tuoyan Analytical Technology Company (GTATC) in Guangzhou according to the laboratory procedure. In this process, approximately 50–100 mg of the powdered sample was placed within a stainless-steel-lined PTFE bomb, accompanied by 1 mL of HF and 1 mL of HNO_3. The sealed bombs underwent heating at 185 °C for 36 h. Following cooling, the bombs were evaporated to dryness on a hot plate. Subsequently, 0.5 mL of HCl was added, the solution was evaporated to dryness once again, and 4 mL of 0.6 M HCl was introduced. The sealed bombs were placed in an oven at 135 °C for 5 h to dissolve any remaining residues. The resultant solution underwent centrifugation at 3000 rpm for 2 min, and the supernatant was loaded into pre-conditioned columns (8 × 110 mm) containing AG 50 W-X2 cation exchange resin for the separation of matrix elements Sr and Rb using 0.6 M HCl. Subsequently, light rare earth elements (REEs) were eluted using 6 mL of 6 M HCl. The solution obtained was then evaporated to dryness, dissolved in 1 mL of 0.17 M HCl, and loaded into pre-conditioned columns containing Ln resin for the separation of Nd from Sm. The measurement of $^{143}Nd/^{144}Nd$ ratios was carried out using a Neptune multicollector (MC)–ICP–MS (Agilent Technologies Inc., Palo Alto, CA, USA). JMC-Nd was analyzed as a standard [7] for $^{143}Nd/^{144}Nd$ ratios. $^{143}Nd/^{144}Nd$ ratios of the JMC-Nd were determined as 0.511587 ± 10.

4. Results

4.1. Whole Rock Major and Trace Element Data

The Laojunshan medium- to coarse-grained and fine-grained muscovite-bearing granites display similar major elemental components. These granites showcase high SiO_2 content ranging from 73.0 to 76.9 wt.%, alongside low levels of MgO (0.14 to 0.30 wt.%), $Fe_2O_3{}^t$ (0.67 to 1.51 wt.%), TiO_2 (0.09 to 0.21 wt.%), and P_2O_5 (0.21 to 0.25 wt.%) contents (Table 1). The entire set of samples falls within the category of weakly peraluminous rocks, ACNK values (molar $Al_2O_3/(CaO + Na_2O + K_2O)$) ranging from 1.00 to 1.06 (see Table 1 and Figure 4a). Additionally, these samples exhibit notable levels of K_2O contents and plot in the fields of the high-K calc-alkaline series and shoshonite series fields (see Figure 4b).
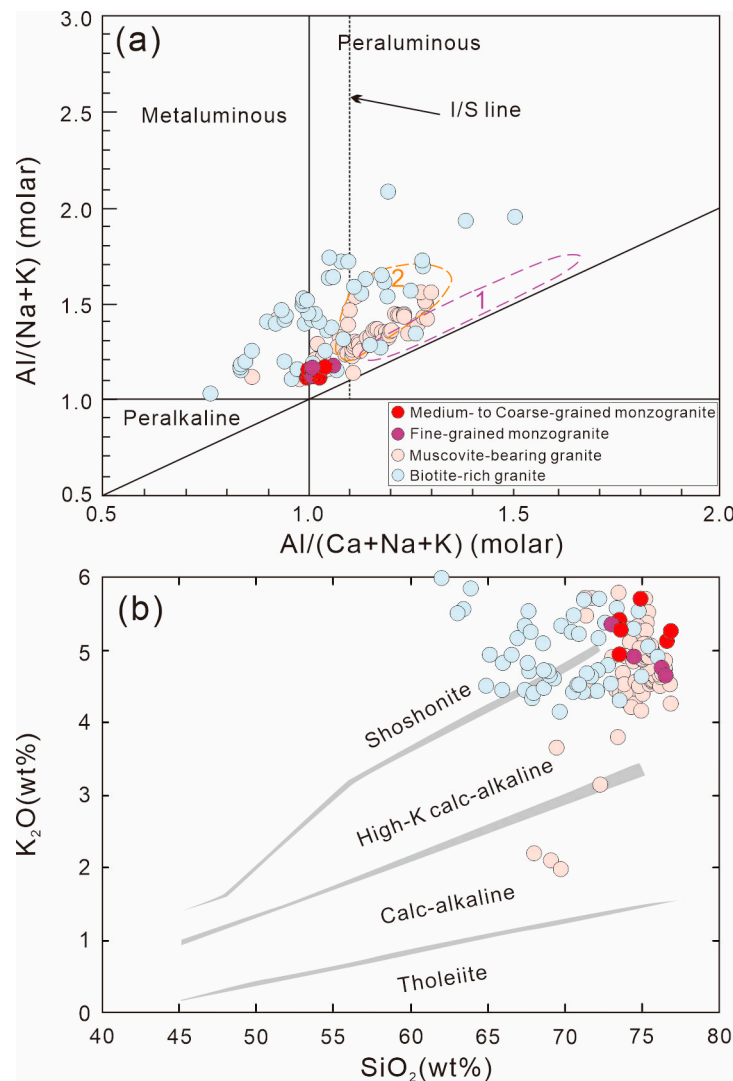
Figure 4. (**a**) Al/(Ca + Na + K) vs. Al/(Na + K) and (**b**) SiO_2 vs. K_2O diagrams. Data of muscovite-bearing granites are from the Late Cretaceous muscovite-bearing peraluminous granitic intrusion in the Youjiang basin, including the Gaofengshan [34], Kafang–Laochang [23,24], Laojunshan [18], Songshujiao [24], Longxianggai [25], and Mangchang [25] intrusions. Data of the biotite-rich granites are from the Jiasha monzogranite [35], Bozhushan episode 1 granite [36], Longchahe [27] granite, and Shenxianshui granite [37]. The fields of the following experimental melts are also shown: ① vapor-absent partial melts of a natural metapelitic rock [38]; and ② melts of a synthetic metapsammitic rock [39].

Uniform trace element characteristics are observed across all samples. The chondrite-normalized rare earth element (REE) diagrams reveal enrichment in LREEs in relation to HREEs (La/Yb$_n$ values of 7.6 to 21.2) and consistent negative Eu anomalies (δEu ranging from 0.26 to 0.39; Figure 5a). In the primitive mantle (PM)-normalized diagrams, all samples show significant negative anomalies in Ba, Sr, Nb, and Ti, coupled with positive anomalies in Rb, K, and Pb (Figure 5b).
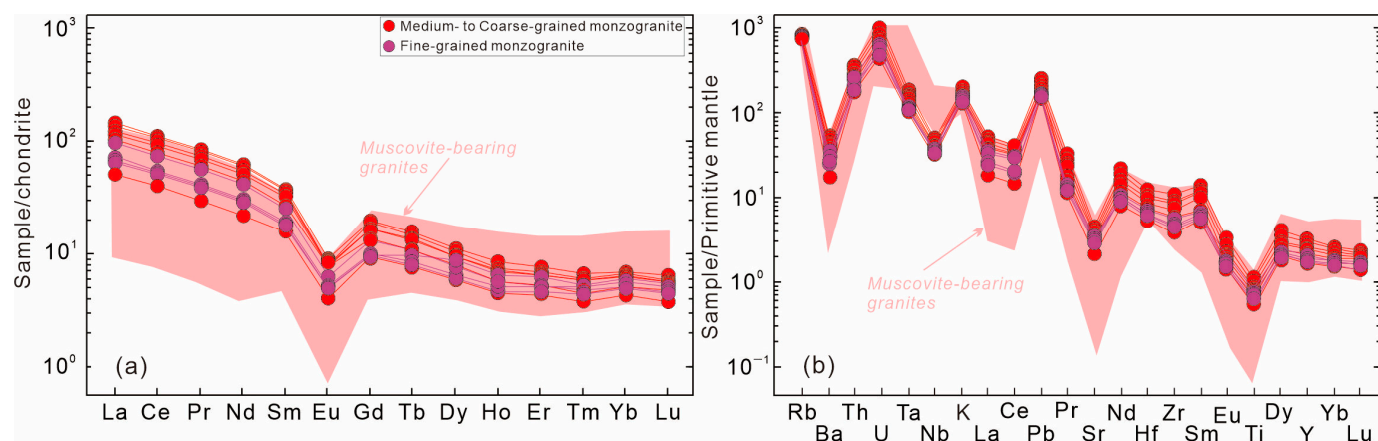
Figure 5. Chondrite-normalized [40] REE patterns (**a**) and primitive mantle-normalized [40] trace element patterns (**b**) for the Laojunshan samples. Data of the Late Cretaceous muscovite-bearing peraluminous granitic intrusion in the Youjiang basin are the same as those shown in Figure 4.

Table 1. Whole-rock major element (wt.%) and trace elements (ppm) contents of the Laojunshan samples.

Sample No.	DL-34	DL-35	DL-36	DL-37	DL-39	DL-44	DL-45	DL-46	DL-49	DL-52
Rock Type	Medium- to Coarse-Grained Monzogranite						Fine-Grained Monzogranite			
SiO$_2$	73.5	73.6	76.6	76.9	74.9	73.5	73	76.5	74.5	76.3
Al$_2$O$_3$	14	13.6	12.4	12.2	13.4	13.7	14.2	12.4	13.6	12.4
Fe$_2$O$_3$t	1.41	1.39	0.85	0.67	0.69	1.51	1.38	1.08	0.89	0.98
MgO	0.28	0.26	0.26	0.18	0.14	0.3	0.27	0.16	0.18	0.19
CaO	0.79	0.9	0.63	0.64	0.74	1.05	0.76	0.63	0.81	0.76
Na$_2$O	3.68	3.82	3.24	3.1	3.53	3.94	3.79	3.61	3.94	3.43
K$_2$O	5.42	5.27	5.12	5.25	5.7	4.94	5.34	4.65	4.91	4.75
MnO	0.04	0.04	0.02	0.02	0.02	0.05	0.05	0.03	0.04	0.04
TiO$_2$	0.18	0.18	0.21	0.14	0.14	0.21	0.16	0.09	0.12	0.12
P$_2$O$_5$	0.24	0.25	0.25	0.23	0.22	0.21	0.22	0.22	0.24	0.22
LOI	0.31	0.52	0.35	0.46	0.49	0.56	0.53	0.51	0.6	0.56
Total	99.8	99.82	99.85	99.8	99.98	99.89	99.79	99.86	99.76	99.79
ACNK	1.04	1.00	1.03	1.02	1.00	1.00	1.06	1.02	1.02	1.02
Sn	16.7	15.8	18.2	31.7	17.1	16.3	20.4	27.5	18.9	19.7
Cu	1.66	1.45	1.66	19	3.57	2.97	6.47	14.6	4.5	9.16
Zn	36.8	36.1	28.7	68.2	23.5	45.5	34.1	31.3	35.3	32.9
Ga	26.8	25.8	26.2	25	23.6	24.5	28.1	25.4	25.4	24.9

Sample No.	DL-34	DL-35	DL-36	DL-37	DL-39	DL-44	DL-45	DL-46	DL-49	DL-52
Rock Type	Medium- to Coarse-Grained Monzogranite					Fine-Grained Monzogranite				
Rb	450	459	444	507	463	441	487	445	470	433
Sr	65.4	57.8	58.1	49.4	81.5	77.2	72.4	38.9	65.4	65.9
Y	11.8	11.4	12.6	7.47	9.01	13.8	11.1	11.7	8.89	8.1
Zr	86.9	89.1	110	39.5	87.2	108	73.1	46.2	57.8	61
Nb	26.3	25.8	27.3	20.8	19.4	25	30	25.1	27.3	22.7
Ba	227	210	225	152	305	252	192	96.2	181	226
La	27.3	28.6	31.4	15.3	24.5	33.6	22.7	11.8	17.1	16
Ce	55.8	58.1	64.7	31.5	48.8	68	45.4	24.3	33.5	32.3
Pr	6.44	6.75	7.53	3.53	5.61	7.79	5.18	2.71	3.87	3.69
Nd	23.5	24.6	27.6	13	20.2	28.5	18.7	9.85	14.1	13.4
Sm	4.65	4.93	5.47	2.65	3.96	5.6	3.66	2.27	2.82	2.65
Eu	0.42	0.42	0.41	0.27	0.45	0.5	0.34	0.22	0.28	0.28
Gd	3.34	3.46	3.82	1.88	2.74	3.96	2.57	1.95	2	1.89
Tb	0.48	0.49	0.53	0.28	0.39	0.57	0.39	0.35	0.3	0.28
Dy	2.33	2.32	2.53	1.43	1.88	2.76	1.98	2.13	1.61	1.44
Ho	0.39	0.38	0.41	0.24	0.31	0.46	0.35	0.38	0.28	0.26
Er	1.05	1	1.11	0.68	0.83	1.24	1.01	1.01	0.82	0.75
Tm	0.14	0.13	0.14	0.09	0.11	0.16	0.15	0.15	0.12	0.11
Yb	0.97	0.92	1.02	0.69	0.79	1.13	1.07	1.06	0.9	0.83
Lu	0.13	0.12	0.14	0.09	0.11	0.16	0.15	0.15	0.13	0.12
Hf	2.77	2.92	3.37	1.47	2.66	3.42	2.4	1.75	1.99	2.11
Ta	6.08	5.17	4.99	4.27	3.94	4.67	6.71	6.02	5.9	5.76
Pb	38.3	38.2	36.9	26.1	40.3	40.6	39.7	27	34.2	30.5
Th	22.9	24.1	27.2	13.5	20.5	27.8	18.9	10.2	15	15.7
U	9.88	12.1	14	18.4	10.5	20.8	23	20.4	18.1	15.2
Rb/Sr	6.9	7.9	7.6	10.3	5.7	5.7	6.7	11.4	7.2	6.6
Zr/Hf	31	31	33	27	33	32	30	26	29	29
Nb/Ta	4.3	5	5.5	4.87	4.92	5.35	4.47	4.17	4.63	3.94
K/Rb	100	95	96	86	102	93	91	87	87	91
T_{Zr}(°C)	742	738	763	684	740	752	729	695	709	714

Note: LOI = loss on ignition. ACNK = molar $Al_2O_3/(CaO + Na_2O + K_2O)$. T_{zr} = 12,900/(2.95 + 0.85M + ln[D_{Zr} zircon/melt]), where D_{Zr} zircon/melt is the ratio of Zr concentration (ppm) in zircon to that in the saturated melt [41].

4.2. Whole Rock Sm–Nd Isotopes

The entire sample set demonstrates enriched and evolved Sm–Nd isotopic compositions, indicated by $\varepsilon_{Nd}(t)$ values within the range of −13.8 to −11.2. These granites exhibit Paleoproterozoic two-stage Nd model ages (T_{2DM}) spanning from 1.80 to 2.01 Ga (refer to Table 2).

Table 2. Whole-rock Sm-Nd isotopic compositions of the Laojunshan samples.

| Sample No.	DL-34	DL-35	DL-36	DL-37	DL-39	DL-44	DL-45	DL-46	DL-49	DL-52
Rock Type	Medium- to Coarse-Grained Monzogranite						Fine-Grained Monzogranite			
$^{147}Sm/^{144}Nd$	0.119554	0.121086	0.119745	0.123164	0.118447	0.11872	0.118255	0.139242	0.12084	0.119487
$^{143}Nd/^{144}Nd$	0.511916	0.511915	0.51189	0.511889	0.511941	0.511976	0.51194	0.512001	0.512006	0.512017
$\pm 2\sigma$	0.000003	0.000002	0.000004	0.000004	0.000003	0.000003	0.000004	0.000003	0.000003	0.000004
$\varepsilon_{Nd}(t)$	−13.2	−13.2	−13.7	−13.8	−12.7	−12	−12.7	−11.8	−11.5	−11.2
T_{2DM}(Ga)	1.9647	1.9672	2.0057	2.0096	1.9234	1.8679	1.9247	1.8482	1.823	1.8046

5. Discussion

5.1. Genetic Type

The Laojunshan medium- to coarse-grained and fine-grained muscovite-bearing granites exhibit weakly peraluminous characteristics, as indicated in Figure 4a. Previous studies based on their high ACNK values (>1.0) suggested that these granites belong to the S-type defined by Chappell and White (1974) [42] and are derived from metasedimentary rocks [9,18]. However, the Laojunshan granites lack typical aluminous minerals of S-type granites, such as garnet and cordierite. Experimental investigations involving metasedimentary rocks have further proposed that the resulting melts are predominantly strongly peraluminous [38,39] (Figure 4). The weakly peraluminous compositions of the Laojunshan samples do not align with these findings (Figure 4a). Additionally, certain samples display slightly higher $\varepsilon_{Nd}(t)$ values than the Precambrian basement, suggesting the involvement of juvenile compositions in the genesis of the Laojunshan granites (Figure 6).
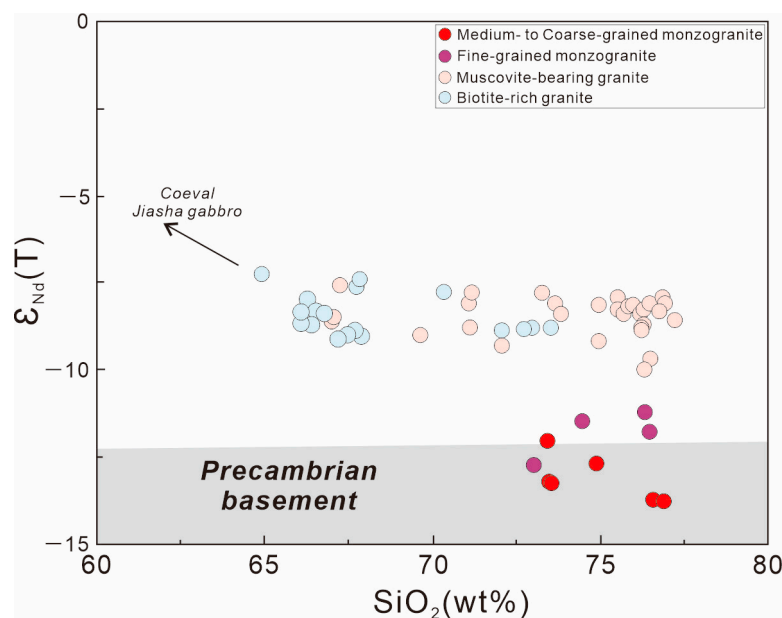
Figure 6. SiO_2 vs. $\varepsilon_{Nd}(t)$ for the Laojunshan granitic samples. Data of the muscovite-bearing granites in Youjiang Basin are the same as those shown in Figure 4. Data of biotite-rich granites in the Youjiang basin are from the Bozhushan medium-grained biotite monzogranite (episode 1) [26] and Longchahe granite [27]; Data on the Precambrian basement is from [26].

Sedimentary sources of S-type granites primarily consist of pelite and psammite. Pelitic rocks are rich in clay but poor in plagioclase, in contrast to psammitic rocks (Sylvester, 1998). Thus, Sylvester (1998) [43] suggested that strongly peraluminous melts derived from pelites exhibit lower CaO/Na_2O ratios (<0.3) and higher Rb/Sr ratios (>2) compared to those from psammites. Based on an average CaO/Na_2O ratio of (0.25) and an average

Rb/Sr ratio [12], Xu et al. (2015) [9] argued that the Laojunshan muscovite-bearing granites belong to the S-type and originated from the partial melting of metamorphosed pelitic rocks in the Precambrian basement. Notably, the Laojunshan samples generally have high FeO^T/MgO ratios (Figure 7a) and exhibit lower $FeO^T + MgO + TiO_2$ contents compared to the experimental melts of metasedimentary and metaigneous rocks (Table 1 and Figure 7b). These geochemical characteristics suggest that the Laojunshan muscovite-bearing granites are products of highly magmatically fractionated processes. In these highly fractionated granites, plagioclase plays a pivotal role as the main differentiated mineral. The low CaO content, coupled with the presence of negative Sr and Eu anomalies, supports the notion of plagioclase removal during the magmatic evolution (Table 1 and Figure 5). The differentiation of the plagioclase led to changes in the CaO/Na_2O ratio within the residual melts. Since Sr is compatible with plagioclase, while Rb is incompatible, the removal of plagioclase increases the Rb/Sr ratio of the resulting melts. The low CaO/Na_2O and high Rb/Sr ratios observed in the Laojunshan granites can be attributed to the magmatic evolution resulting from plagioclase differentiation. To summarize, the Laojunshan monzogranites are highly fractionated and do not fall into the category of typical S-type granites.
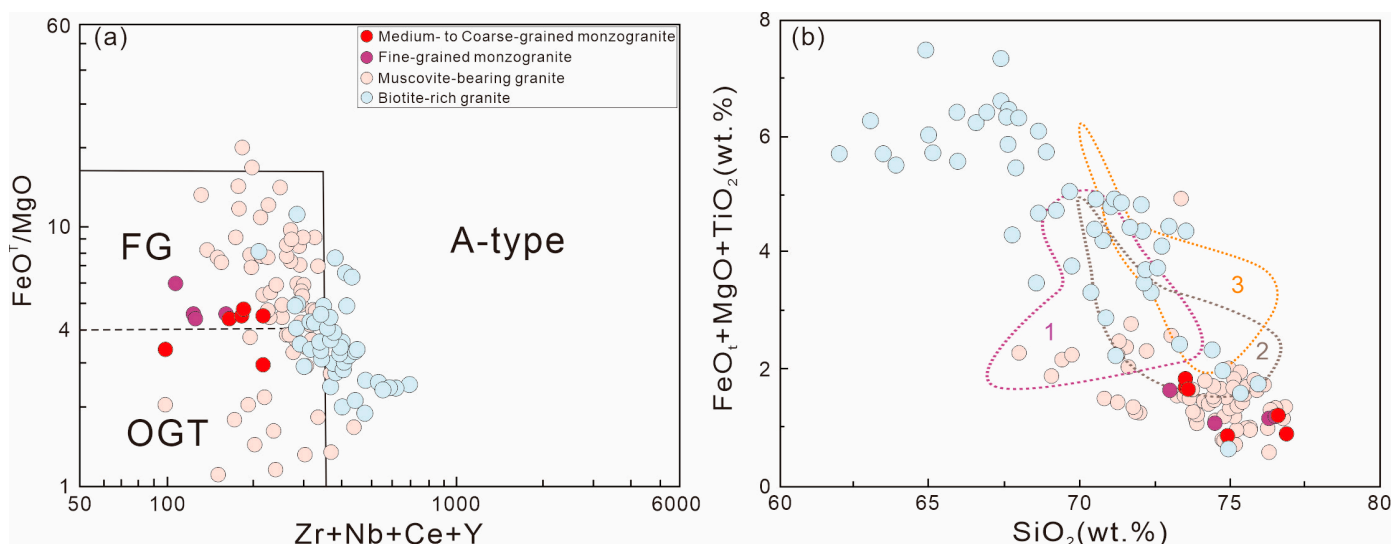
Figure 7. (**a**) Zr + Nb + Ce + Y vs. FeO^T/MgO (modified after [44]) and (**b**) SiO_2 vs. $FeO^t + MgO + TiO_2$ diagrams. Data of the muscovite-bearing granites are the same as those shown in Figure 4. Data of the biotite-rich granites are from the Jiasha monzogranite [35], Bozhushan episode 1 granite [36], Longchahe [27] granite, and Shenxianshui granite [37]. The fields of some experimental melts are also shown in the context, including vapor-absent partial melts of ① a two-mica schist (plagioclase-poor natural metapelitic rock; [38]); ② a biotite gneiss (plagioclase-rich synthetic metapsammitic rock; [39]); and ③ a quartz amphibolite [38,39]. Abbreviations: FG, fractionated granites; OGT, I-, S-, and M-type granites.

### 5.2. Petrogenesis of the Laojunshan Monzogranites

In the context of the Youjiang Basin, the Late Cretaceous biotite-bearing granites exhibited lower FeO^T/MgO ratios (Figure 7a) and higher $FeO_t + MgO + TiO_2$ contents (Figure 7b) than the coeval muscovite-bearing granites. In contrast to the biotite-bearing granites, the Laojunshan muscovite-bearing granites manifest higher SiO_2 levels and lower CaO, Al_2O_3, MgO, $Fe_2O_3^T$, and TiO_2 contents (Figure 8), indicating the differentiation of biotite and plagioclase. In the REE and PM-normalized diagrams, the negative Eu, Ba, Sr, and Ti anomalies also align with the differentiation of these two minerals (Figure 5). Accessory minerals found in the Laojunshan granites encompass titanite, apatite, zircon, and sphene. A coherent decreasing trend in SiO_2 vs. P_2O_5 is absent, arguing against the differentiation of apatite (Figure 8e).
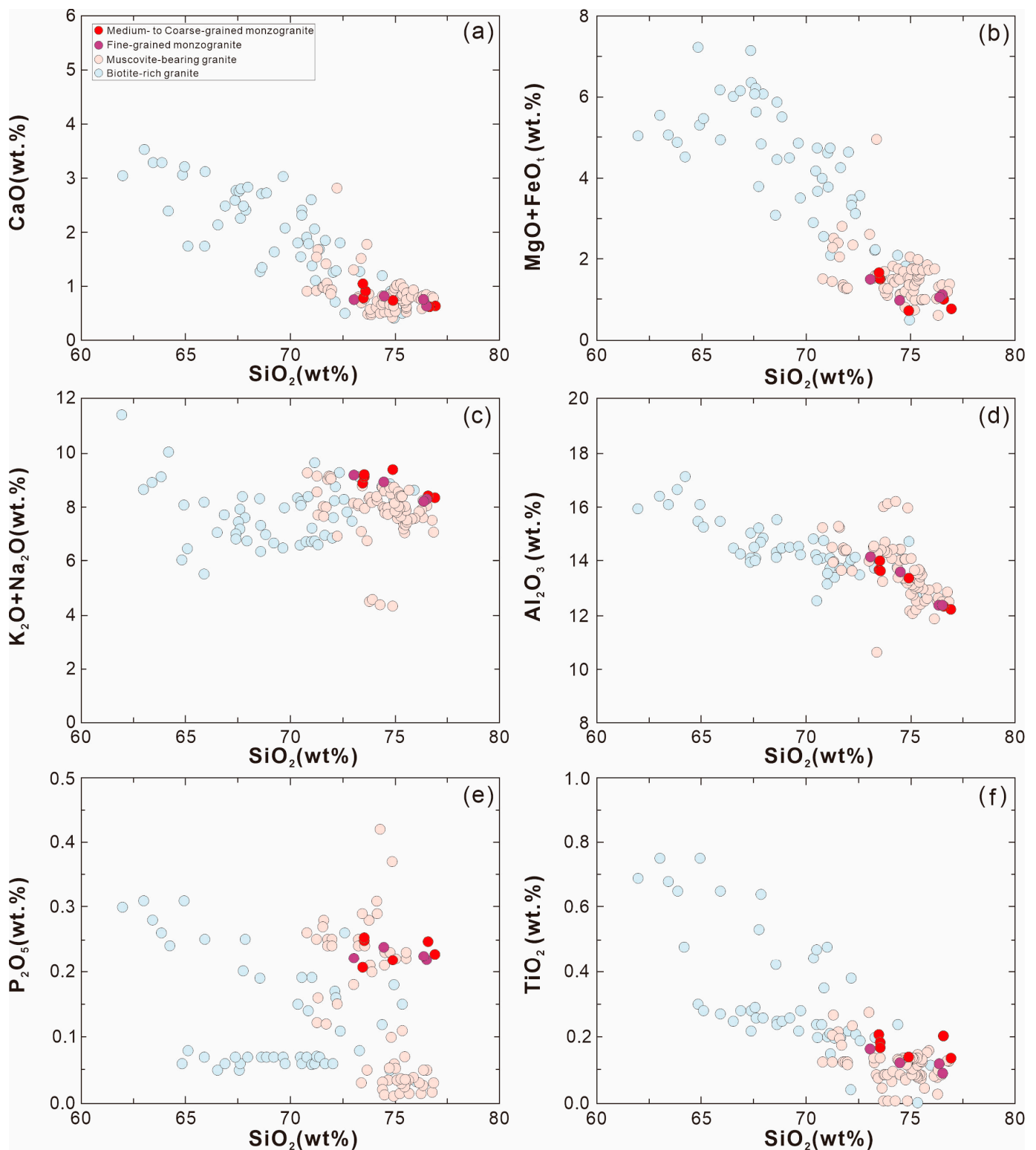
Figure 8. Harker diagrams of the Laojunshan granites, muscovite-bearing granites, and biotite-rich granites in the Youjiang Basin. Other data are the same as those shown in Figure 7.

Nb and Ta are strongly compatible with ilmenite and sphene, respectively. Studies on the partition coefficients have revealed that Ta is more compatible than Nb in these two minerals ($D^{Nb} < D^{Ta}$) [45]. If ilmenite and sphene differentiation were to occur, melt Nb and Ta contents should decrease while the Nb/Ta ratio increases [46]. This is exactly

opposite to the trend of magmatic evolution (Figure 9b). A decreasing Zr content, coupled with a declining Zr/Hf ratio, indicates zircon differentiation (Figure 9a).
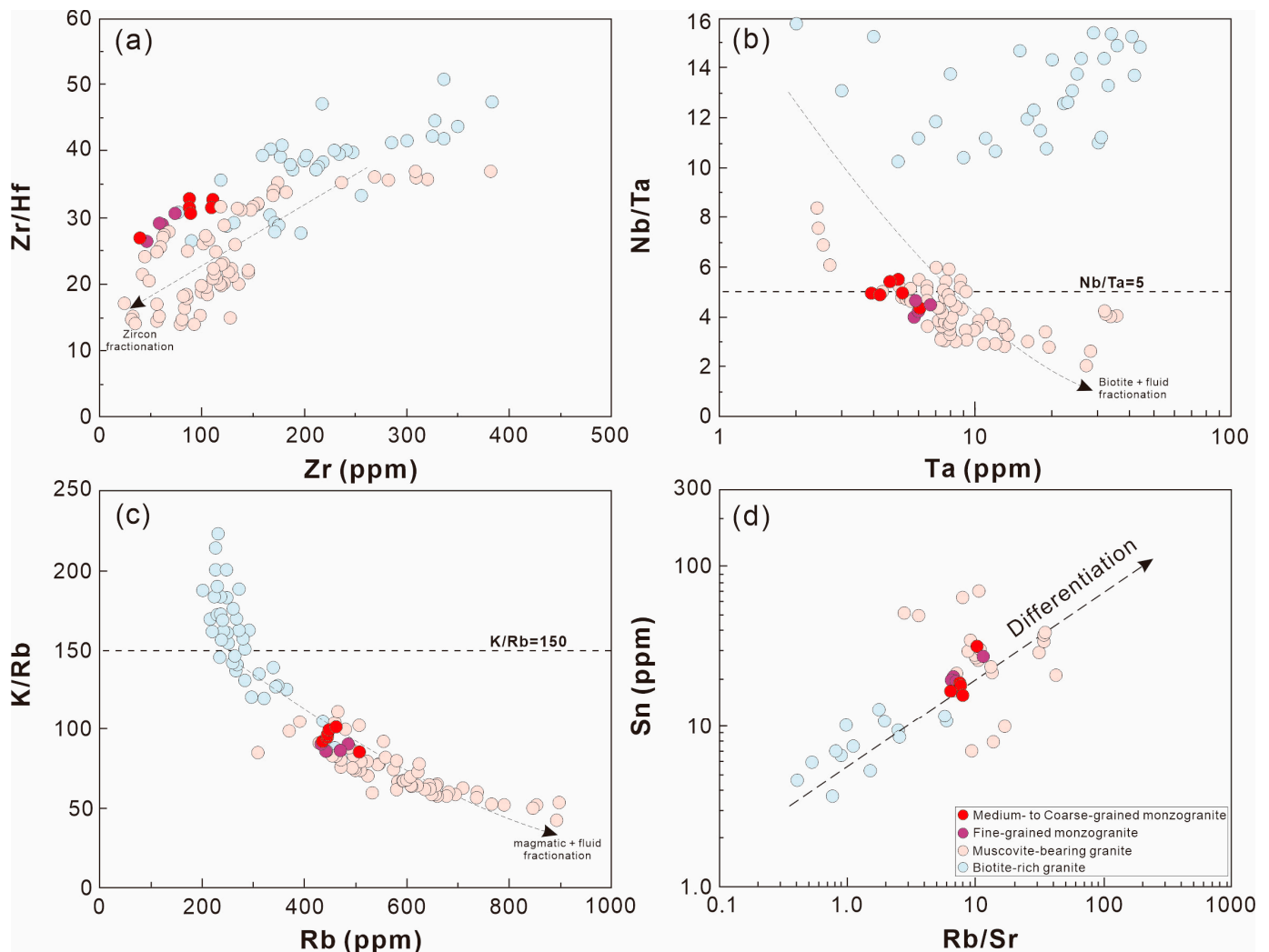

Figure 9. (**a**) Zr vs. Zr/Hf, (**b**) Ta vs. Nb/Ta, (**c**) Rb vs. K/Rb, and (**d**) Rb/Sr vs. Sn diagrams.

Remarkably, the Laojunshan muscovite-bearing monzogranites display extremely low Nb/Ta ratios ranging from 3.9 to 5.5. Although the differentiation of biotite can contribute to a reduced Nb/Ta ratio, prior modeling indicates that an improbable differentiation of biotite of more than 50% would be required to achieve an Nb/Ta ratio of <5 [47]. Hence, magmatic differentiation alone is insufficient to explain the observed low Nb/Ta ratios. Collating geochemical data from tin-bearing granites associated with Sn, W, and/or U deposits, Ballouard et al. (2016) [47] proposed that an Nb/Ta ratio of approximately 5 is a critical marker for identifying the magmatic–hydrothermal transition. Shaw (1968) [48] also suggested that low K/Rb ratios below 150 indicate fluid exsolution from a granitic magmatic chamber. The low K/Rb (86 to 102) and Nb/Ta (3.9 to 5.5) ratios in our samples indicate that the Laojunshan muscovite-bearing granites underwent fluid exsolution (Figure 9b,c). Experimental studies investigating the partitioning of Nb and Ta between the fluid and granitic melt have demonstrated that $D^{\text{fluid/melt}}$ values for Nb/Ta exceed 1 [49], confirming that fluid exsolution further contributed to the decrease in the Nb/Ta ratio within the Laojunshan muscovite-bearing granites. To summarize, the genesis of Laojunshan muscovite-bearing granites can be attributed to mineral differentiation (Bt + Pl + Zrn) and the fluid exsolution of crust-derived melts.

5.3. Implications for Tin Mineralization in the Youjiang Basin

In terms of tin content, granites can be classified into tin-bearing granites (>15 ppm) and tin-barren granites (<15 ppm) [50]. Most primary Sn deposits worldwide are associated with the latest crystallized muscovite-bearing granites containing high tin contents (>15 ppm) and exhibiting highly evolved compositions [1,2]. By employing Harker diagrams of Ti vs. Sn, Rb/Sr vs. Sn, and Ta vs. Sn, previous research suggested that muscovite-bearing granites can be generated through the extreme differentiation of crust-derived melts [1,3,7,14]. Through a comparison of element partitioning between leucosomes and resites of high- and low-temperature migmatites, Wolf et al. (2018) [10] proposed that the complete consumption of high-temperature (>800 °C) anatexis involving biotite produces tin-bearing peraluminous granites with less fractionation through a vapor-absent melting reaction. During the high-temperature melting, Sn-hosts (biotite) become unstable, and the resulting melts enriched in Sn enrichment [10]. The zircon saturation temperatures of the samples ranged from 684 °C to 763 °C (Table 1). Unlike coeval biotite granites in the Youjiang Basin, the Laojunshan muscovite-bearing granites do exhibit lower zircon saturation temperatures (Figure 10). Consequently, the Laojunshan muscovite-bearing granites characterized by high tin contents (15.8 to 31.7 ppm) were not formed through the high-temperature melting of crustal rocks. In comparison to Late Cretaceous biotite-rich granites in the Youjiang Basin, the Laojunshan muscovite-bearing granites display more evolved compositions in terms of whole-rock major and trace element contents (Figures 7–9). Within the Harker diagram of Rb/Sr vs. Sn, the tin content in the Laojunshan monzogranites increased during magmatic differentiation (Figure 9d). In conclusion, we propose that the enrichment of tin in the Laojunshan granites is linked to magmatic differentiation.
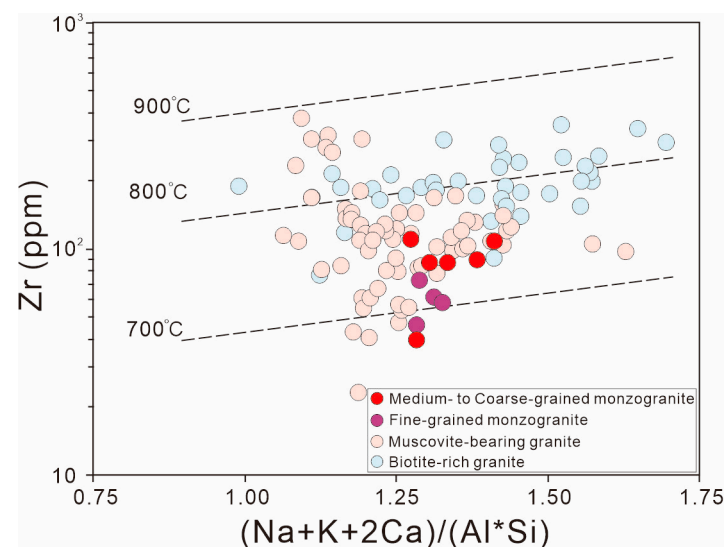
Figure 10. (Na + K + 2Ca)/(Al*Si) vs. Zr diagram (modified after [41]). Other data are the same as those shown in Figure 7.

The Youjiang Basin of the South China Block hosts numerous large and super-large Late Cretaceous tin-polymetallic deposits, including the Gejiu, Dulong, Bainiuchang, Dachang, and Mangchang deposits. Prior investigations have established an association between these deposits and coeval Kafang–Laochang, Songshujiao, Laojunshan, Bozhushan, Longxianggai, and Machang muscovite-bearing granites [15–18,20]. Other muscovite-bearing granites exhibit nearly identical major and trace element geochemical characteristics as the Laojunshan granites, including a peraluminous composition, enrichment in K_2O (Figure 4b), high FeO^T/MgO ratios (Figure 7b), low CaO and Al_2O_3 (Figure 8), low $FeO^t + MgO + TiO_2$ (Figure 7b), and low Zr/Hf and K/Rb ratios (Figure 9). These similarities imply that all of the muscovite-bearing peraluminous granites were produced through mineral differentiation and fluid exsolution of crust-derived melts. Late Cretaceous

biotite-rich granites also occurred in the Youjiang Basin, such as the Bozhushan biotite monzogranite (episode 1), Jiasha monzogranite, Longchahe monzogranite, and Shenxianshui granite [26,27]. These biotite-rich granites exhibit the same enriched Sm–Nd isotopic compositions as the muscovite-bearing granites (except for Laojunshan; Figure 6), suggesting that they share a common crustal source. In comparison to the muscovite-bearing granites, biotite-rich granites display less evolved compositions, characterized by lower SiO_2 contents and higher $FeO_t + MgO + TiO_2$ and FeO^T/MgO ratios (Figure 7 and Table 1). Within the Harker diagram of Rb/Sr vs. Sn, the Sn content in muscovite-bearing and biotite-rich granites increases significantly during the course of magmatic differentiation (Figure 9d). To sum up, we conclude that the muscovite-bearing peraluminous granites were derived from the mineral differentiation and fluid exsolution of crust-derived melts rather than the direct melting of metasedimentary rocks.

6. Conclusions

(1) The Laojunshan medium- to coarse-grained and fine-grained muscovite-bearing peraluminous granites exhibit geochemical characteristics that are indicative of highly fractionated compositions.

(2) These granites were the result of mineral differentiation (involving Biotite + Plagioclase + Zircon) and fluid exsolution of crust-derived melts during the process of magmatic evolution.

(3) The entirety of muscovite-bearing peraluminous granites found in the Youjiang Basin have been formed through the processes of mineral differentiation and fluid exsolution of crust-derived melts subsequent to partial melting, rather than originating directly from the melting of metasedimentary rocks.

(4) The Late Cretaceous tin mineralization in the Youjiang Basin was controlled by extreme differentiation and fluid exsolution.

Author Contributions: Conceptualization, P.L. and L.L.; methodology, P.L.; formal analysis, L.L., P.L. and X.L.; investigation, P.L., X.L. and L.L.; data curation, P.L., X.L. and L.L.; writing—original draft, P.L.; writing—review & editing, X.L. and L.L.; supervision, X.L. and L.L.; Project administration, X.L. All authors have read and agreed to the published version of the manuscript.

References

1. Lehmann, B. Tin granites, geochemical heritage, magmatic differentiation. *Geol. Rundsch.* **1987**, *76*, 177–185. [CrossRef]
2. Lehmann, B. *Metallogeny of Tin*; Springer: Berlin/Heidelberg, Germany, 1990; p. 211.
3. Lehmann, B. Formation of tin ore deposits: A reassessment. *Lithos* **2021**, *402–403*, 105756. [CrossRef]
4. Barbarin, B. Genesis of the two main types of peraluminous granitoids. *Geology* **1996**, *24*, 295–298. [CrossRef]
5. Jiang, Y.-H.; Zhu, S.-Q. Petrogenesis of the Late Jurassic peraluminous biotite granites and muscovite-bearing granites in SE China: Geochronological, elemental and Sr-Nd-O-Hf isotopic constraints. *Contrib. Mineral. Petrol.* **2017**, *172*, 101. [CrossRef]
6. Zhou, X.; Sun, T.; Shen, W.; Shu, L.; Niu, Y. Petrogenesis of Mesozoic granitoids and volcanic rocks in South China: A response to tectonic evolution. *Episodes* **2006**, *29*, 26–33. [CrossRef] [PubMed]
7. Liu, Z.; Tan, S.C.; Wang, G.C.; Li, M.L.; He, X.H.; Zhang, Y.H. Peraluminous granite related to tin mineralization formed by magmatic differentiation and fluid exsolution of metaluminous melt: A case study from the Bozhushan batholith, South China Block. *Ore Geol. Rev.* **2022**, *150*, 105148. [CrossRef]

8. Romer, R.L.; Kroner, U. Sediment and weathering control on the distribution of Paleozoic magmatic tin–tungsten mineralization. *Miner. Deposita* **2015**, *50*, 327–338. [CrossRef]
9. Xu, B.; Jiang, S.Y.; Wang, R.; Ma, L.; Zhao, K.D.; Yan, X. Late Cretaceous granites from the giant Dulong Sn-polymetallic ore district in Yunnan Province, South China: Geochronology, geochemistry, mineral chemistry and Nd–Hf isotopic compositions. *Lithos* **2015**, *218–219*, 54–72. [CrossRef]
10. Wolf, M.; Romer, R.L.; Franz, L.; López-Moro, F.J. Tin in granitic melts: The role of melting temperature and protolith composition. *Lithos* **2018**, *310–311*, 20–30. [CrossRef]
11. Patiño Douce, A.E.; Harris, N. Experimental Constraints on Himalayan Anatexis. *J. Petrol.* **1998**, *39*, 689–710. [CrossRef]
12. Castro, A.; Patiño Douce, A.E.; Guillermo Corretgé, L.; de la Rosa, J.D.; El-Biad, M.; El-Hmidi, H. Origin of peraluminous granites and granodiorites, Iberian massif, Spain: An experimental test of granite petrogenesis. *Contrib. Mineral. Petrol.* **1999**, *135*, 255–276. [CrossRef]
13. Boissavy-Vinau, M.; Roger, G. The TiO2/Ta ratio as an indicator of the degree of differentiation of tin granites. *Miner. Depos.* **1980**, *15*, 231–236. [CrossRef]
14. Lehmann, B. Metallogeny of tin; magmatic differentiation versus geochemical heritage. *Econ. Geol.* **1982**, *77*, 50–59. [CrossRef]
15. Li, K.W.; Zhang, Q.; Wang, D.P.; Cai, Y.; Liu, Y.P. LA-MC-ICP-MS U-Pb geochronology of cassiterite from the Bainiuchang polymetallic deposit, Yunnan Province, China. *Acta Mineral. Sin.* **2013**, *33*, 203–209, (In Chinese with English abstract).
16. Guo, J.; Zhang, R.Q.; Sun, W.D.; Ling, M.X.; Hu, Y.B.; Wu, K.; Luo, M.; Zhang, L. Genesis of tin-dominant polymetallic deposits in the Dachang district, South China: Insights from cassiterite U–Pb ages and trace element compositions. *Ore Geol. Rev.* **2018**, *95*, 863–879. [CrossRef]
17. Guo, J.; Zhang, R.Q.; Li, C.Y.; Sun, W.D.; Hu, Y.B.; Kang, D.M.; Wu, J.D. Genesis of the Gaosong Sn–Cu deposit, Gejiu district, SW China: Constraints from in situ LA-ICP-MS cassiterite U–Pb dating and trace element fingerprinting. *Ore Geol. Rev.* **2018**, *92*, 627–642. [CrossRef]
18. Zhao, Z.Y.; Hou, L.; Ding, J.; Zhang, Q.M.; Wu, S.Y. A genetic link between Late Cretaceous granitic magmatism and Sn mineralization in the southwestern South China Block: A case study of the Dulong Sn-dominant polymetallic deposit. *Ore Geol. Rev.* **2018**, *93*, 268–289. [CrossRef]
19. Mao, J.W.; Ouyang, J.G.; Song, S.W.; Santosh, M.; Yuan, S.D.; Zhou, Z.H.; Zheng, W.; Liu, H.; Liu, P.; Cheng, Y.B.; et al. Geology and Metallogeny of Tungsten and Tin deposits in China. *Soc. Econ. Geol. Spec. Publ.* **2019**, *22*, 411–482.
20. Cheng, Y.B.; Mao, J.W.; Spandler, C. Petrogenesis and geodynamic implications of the Gejiu igneous complex in the western Cathaysia block, South China. *Lithos* **2013**, *175–176*, 213–229. [CrossRef]
21. Sun, W. Initiation and evolution of the South China Sea: An overview. *Acta Geochim.* **2016**, *35*, 215–225. [CrossRef]
22. Guo, J.; Wu, K.; Seltmann, R.; Zhang, R.; Ling, M.; Li, C.; Sun, W. Unraveling the link between mantle upwelling and formation of Sn-bearing granitic rocks in the world-class Dachang tin district, South China. *Geol. Soc. Am. Bull* **2022**, *134*, 1043–1064. [CrossRef]
23. Cheng, Y.B.; Mao, J.W.; Xie, G.Q.; Chen, M.H.; Zhao, C.S.; Yang, Z.X.; Zhao, H.J.; Li, X.Q. Petrogenesis of the Laochang-Kafang Granite in the Gejiu Area, Yunnan Province: Constraints from geochemistry and zircon U-Pb dating. *Acta Geol. Sin.* **2008**, *82*, 1476–1493, (In Chinese with English abstract).
24. Liu, Y.; Zhang, L.; Mo, X.; Santosh, M.; Dong, G.; Zhou, H. The giant tin polymetallic mineralization in southwest China: Integrated geochemical and isotopic constraints and implications for Cretaceous tectonomagmatic event. *Geosci. Front.* **2020**, *11*, 1593–1608. [CrossRef]
25. Wu, J.; Yuan, H.W.; Gan, N.J.; Wei, S.C.; Liao, J.; Zhang, J.; Liang, H.Y. Source characteristics of magmatic rocks and zircon U-Pb age in the Mangchang ore field, Danchi metallogenic belt, Guangxi. *Acta Petrol. Sin.* **2020**, *36*, 1586–1596, (In Chinese with English abstract). [CrossRef]
26. Wang, G.C.; Liu, Z.; Tan, S.C.; Wang, Y.-K.; He, X.H.; Li, M.L.; Qi, C.S. Petrogenesis of biotite granite with transitional I-A-type affinities: Implications for continental crust generation. *Lithos* **2021**, *396–397*, 106199. [CrossRef]
27. Cheng, Y.; Spandler, C.; Mao, J.; Rusk, B.G. Granite, gabbro and mafic microgranular enclaves in the Gejiu area, Yunnan Province, China: A case of two-stage mixing of crust- and mantle-derived magmas. *Contrib. Mineral. Petrol.* **2012**, *164*, 659–676. [CrossRef]
28. Guo, J. Tin mineralization Events and Fertility of Granitoids in the Youjiang Basin, South China: The Gejiu and Dachang Sn-Polymetallic Districts as Examples. Ph.D. Thesis, University of Chinese Academy of Sciences, Beijing, China, 2019; p. 247.
29. Liu, Y.P.; Ye, L.; Li, C.Y.; Song, B.; Li, T.S.; Guo, L.G.; Pi, D.H. Discovery of the Neoproterozoic magmatics in southeastern Yunnan: Evidence from SHRIMP zircon U-Pb dating and lithogeochemistry. *Acta Petrol. Sin.* **2006**, *22*, 916–926, (In Chinese with English abstract).
30. Liu, J.-S.; Zhang, H.-P.; Ouyang, Y.-F.; Zhang, C.-H. Bainiuchang super-large silver-polymetallic ore deposit related to granitic magmatism in Mengzi, Yunnan. *J. Central South. Univ. Technol.* **2007**, *14*, 568–574. [CrossRef]
31. Yang, G.S.; Wen, H.J.; Ren, T.; Xu, S.H.; Wang, C.Y. Geochronology, geochemistry and Hf isotopic composition of Late Cretaceous Laojunshan granites in the western Cathaysia block of South China and their metallogenic and tectonic implications. *Ore Geol. Rev.* **2020**, *117*, 103297. [CrossRef]
32. Feng, J.; Mao, J.; Pei, R.; Zhou, Z.; Yang, Z. SHRIMP zircon U-Pb dating and geochemical characteristics of Laojunshan granite intrusion from the Wazha tungsten deposit, Yunnan Province and their implications for petrogenesis. *Acta Petrol. Sin.* **2010**, *26*, 845–857, (in Chinese with English abstract).

33. Lan, J.B.; Liu, Y.P.; Ye, L.; Zhang, Q.; Wang, D.P.; Su, H. Geochemistry and age spectrum of late Yanshanian granites from Laojunshan area, southeastern Yunnan province, China. *Acta Mineral. Sin.* **2016**, *36*, 441–454, (In Chinese with English abstract).

34. Li, X.L.; Mao, J.W.; Cheng, Y.B.; Zhang, J. Petrogenesis of the Gaofengshan granite in Gejiu area, Yunnan Province: Zircon U-Pb dating and geochemical constraints. *Acta Petrol. Sin.* **2012**, *28*, 183–198, (In Chinese with English abstract).

35. Jia, R.X. Geological and Geochemical Study of Gejiu Tin Ore Concentration Area in Yunnan. Ph.D. Thesis, Northwest University, Xi'an, China, 2005; p. 150.

36. Xie, H.J.; Zhang, Q.; Zhu, C.H. Petrology and REE-trace element geochemistry of Bozhushan granite pluton in southeastern Yunnan Province, China. *Acta Mineral. Sin.* **2009**, *29*, 481–490, (In Chinese with English abstract). [CrossRef]

37. Chen, W. The Granitic Magmatism and Its Significance of Mineralization in Gejiu, Yunnan. Master's Thesis, China University of Geosciences (Beijing), Beijing, China, 2019; p. 71.

38. Patiño Douce, A.E.; Johnston, A.D. Phase equilibria and melt productivity in the pelitic system: Implications for the origin of peraluminous granitoids and aluminous granulites. *Contrib. Mineral. Petrol.* **1991**, *107*, 202–218. [CrossRef]

39. Patiño Douce, A.E.; Beard, J.S. Dehydration-melting of Biotite Gneiss and Quartz Amphibolite from 3 to 15 kbar. *J. Petrol.* **1995**, *36*, 707–738. [CrossRef]

40. Sun, S.S.; McDonough, W.F. Chemical and isotopic systematics of oceanic basalts: Implications for mantle composition and processes. In *Magmatism in the Ocean. Basin*; Geological Society Special Publication: London, UK, 1989; Volume 42, pp. 313–345. [CrossRef]

41. Watson, E.B.; Harrison, T.M. Zircon saturation revisited: Temperature and composition effects in a variety of crustal magma types. *Earth Planet. Sci. Lett.* **1983**, *64*, 295–304. [CrossRef]

42. Chappell, B.W.; White, A.J.R. Two contrasting granite types. *Pac. Geol.* **1974**, *8*, 173–174.

43. Sylvester, P.J. Post-collisional strongly peraluminous granites. *Lithos* **1998**, *45*, 29–44. [CrossRef]

44. Whalen, J.B.; Currie, K.L.; Chappell, B.W. A-type granites: Geochemical characteristics, discrimination and petrogenesis. *Contrib. Mineral. Petrol.* **1987**, *95*, 407–419. [CrossRef]

45. Xiong, X.; Keppler, H.; Audétat, A.; Ni, H.; Sun, W.; Li, Y. Partitioning of Nb and Ta between rutile and felsic melt and the fractionation of Nb/Ta during partial melting of hydrous metabasalt. *Geochim. Cosmochim. Acta* **2011**, *75*, 1673–1692. [CrossRef]

46. Stepanov, A.; Mavrogenes, J.A.; Meffre, S.; Davidson, P. The key role of mica during igneous concentration of tantalum. *Contrib. Mineral. Petrol.* **2014**, *167*, 1009. [CrossRef]

47. Ballouard, C.; Poujol, M.; Boulvais, P.; Branquet, Y.; Tartèse, R.; Vigneresse, J.L. Nb-Ta fractionation in peraluminous granites: A marker of the magmatic-hydrothermal transition. *Geology* **2016**, *44*, 231–234. [CrossRef]

48. Shaw, D. A review of K-Rb fractionation trends by covariance analysis. *Geochim. Cosmochim. Acta* **1968**, *32*, 573–601. [CrossRef]

49. Chevychelov, V.Y.; Zaraisky, G.P.; Borisovskii, S.E.; Borkov, D.A. Effect of melt composition and temperature on the partitioning of Ta, Nb, Mn, and F between granitic (alkaline) melt and fluorine-bearing aqueous fluid: Fractionation of Ta and Nb and conditions of ore formation in rare-metal granites. *Petrology* **2005**, *13*, 305–321.

50. Barsukov, V.L. The geochemistry of tin, (translated from Geokhimiya 1957: 36–45). *Geochemistry* **1957**, *1*, 41–52.